Molecular Imaging/PET/CT

Simultaneous PET/MRI: Impact on cancer management-A comprehensive review of cases

Amarnath Jena, Sangeeta Taneja, Abhishek Jha

Departments of Molecular Imaging and Nuclear Medicine, Indraprastha Apollo Hospital, Sarita Vihar, Delhi-Mathura Road, New Delhi, India

Correspondence: Dr. Sangeeta Taneja, Departments of Molecular Imaging and Nuclear Medicine, Indraprastha Apollo Hospital, Sarita Vihar, Delhi- Mathura Road, New Delhi - 110 076, India. E-mail: s_taneja1974@yahoo.com

Abstract

The metabolic mapping of malignancy in whole body in a single examination by PET/CT has gained widespread acceptance where the CT provides an anatomical correlate for the PET. MRI offers advantage over CT in providing better anatomical information owing to its high soft tissue resolution especially in brain, liver, neck, pelvis and bone marrow. Simultaneous PET/ MRI is a new multimodal imaging modality that is expected to improve the diagnostic performance of imaging wherein better anatomical and metabolic information can be acquired at the same time and space during a single examination time. Also, MR attributes like diffusion, perfusion and spectroscopy may further add to its diagnostic potential. In this article, we present our initial experience in illustrated cases done with simultaneous PET/MRI and outline its potential for several clinical applications in oncology.

Key words: Fluorodeoxyglucose-positron emission tomography; oncology; simultaneous positron emission tomography/magnetic resonance imaging

Introduction

The metabolic map from positron emission tomography (PET) overlaid on its morphologic correlate from computed tomography (CT) provides an overview of the disease load in the whole body in a single examination and has shown to have immense clinical impact on the diagnostic and therapeutic strategies used for cancer management.[1] Nevertheless, in several instances, magnetic resonance imaging (MRI) is additionally needed with PET/CT for better delineation of lesion, especially in brain, neck, liver, pelvis, bone marrow, and musculoskeletal soft tissues where MRI scores over CT in providing better soft tissue differentiation and characterization.

The need for combining PET with MRI had long been felt and attempts were made to retrospectively fuse PET and MR information acquired at two different time points using dedicated software registration algorithms and extract valuable information provided by these modalities individually. Spatially separated PET and MR systems have been developed with the patient's table moving in which the patient undergoes PET and MR sequentially. However, these approaches are often associated with longer examination times and registration errors due to patient movement and positioning between two different examinations.

With the advent of avalanche photodiodes which are not affected by the strong magnetic field of the MR system, unlike the conventional photomultiplier tubes, it has been possible to bring a PET insert into the MR system which marked the beginning of a revolutionary change in medical diagnostics.

The recently introduced simultaneous PET/MRI, the Biograph mMR (Siemens, Erlangan, Germany), harbors a state-of-the-art avalanche photodiode-based PET system

into the gantry of a 3T MR scanner. The PET images are acquired along with the MR images at the same time, unlike the conventional PET/CT where metabolic and anatomical information are acquired sequentially and misalignment may occur due to physical patient motion or physiological motion of the organs caused by respiration, bowel movement, or filling of the urinary bladder, depending upon the time interval between the acquisitions. Thus, simultaneous PET/MRI combines the metabolic imaging capabilities of PET and the unmatched soft tissue contrast of MRI and appears to be a promising modality for oncologic imaging, its strength being the simultaneity of acquisition which also provides better spatial registration compared to the sequential acquisition of PET and CT.[2,3] The strength of PET/MRI system is also significantly contributed by the MR component, which has attributes like diffusion, perfusion, spectroscopy, and functional imaging in its diagnostic armamentarium. Moreover, with all its potentialities, simultaneous PET/MRI is expected not only to improve the diagnostic potential but also holds promise for better delineation of the target volume in surgical and radiotherapy planning.

In this article, we intend to present a few cases wherein simultaneous PET/MR was done and where the MR component adequately complemented and/or supplemented the information from PET and aided in the differential diagnosis of lesions.

Imaging protocol

This retrospective study was conducted after obtaining approval from the institutional review board. The cases were selected from our initial 217 oncology cases that underwent either primarily simultaneous PET/MRI or as a complementary examination for oncology cases initially referred for PET/CT during the period from January 2013 to June 2013, after taking a written informed consent. A whole body (WB) simultaneous PET/MRI was done on Biograph mMR (Siemens) along with a dedicated study for the region of interest, if required, after injecting single dose of ^{18}F-*fluorodeoxyglucose* (^{18}F-FDG) as radiotracer.

The WB simultaneous PET/MRI was acquired in five bed positions, starting the acquisition from the mid-thigh to the head. Each bed position comprised: A3D coronal 2-point Dixon sequence acquired for 19 sec which was used for generating four different MR images: T1-weighted in-phase, T1-weighted out-phase, and water-only and fat-only images used for attenuation correction; Turbo flash T1 Repetition time (TR) = 1800 ms, Echo time (TE)=2.49 ms, Flip angle (FA) = 20°, Field of view (FOV) = 450 mm, matrix = 1.4 × 1.2 × 5.0, TA = 59 sec, slice = 33, thickness = 5 mm); T2 Short tau inversion recovery (STIR) (TR = 3400 ms, TE = 46.0 ms, FA = 120°, FOV = 450 mm, matrix = 1.9 × 1.4 × 6.0, TA = 1 min 30 sec, slice = 33, thickness = 6 mm); and coronal T2 half-Fourier acquisition single-shot turbo spin-echo (HASTE) (TR = 1200 ms, TE = 72.0 ms, FA = 90°,

FOV = 450 mm, matrix = 1.7 × 1.2 × 6.0, TA = 36 sec, slice = 30, thickness = 6 mm) for anatomical localization and characterisation of the PET uptake. Total MR imaging time per bed position was 3 min 30 sec. The PET acquisition started simultaneously with the Dixon sequence for 4 min per bed position which ensured optimal spatial and temporal correspondence between the MR and PET data.

The protocol also included: T2W FLAIR for brain (TR = 6000, TE = 94, TI = 2026, slice = 5 mm, FOV = 200 × 221, TA = 1 min 12 sec); T2W axial or sagittal for pelvis (TE = 4890, TE = 99, FOV = 252 × 281, slice = 4 mm), diffusion (b values of 50,400,800, FOV 286 × 381, slice = 6 mm) for abdomen and pelvis, and STIR sagittal (TR = 3500, TE = 25, TI = 220, FOV = 643 × 381, slice = 4 mm) for the spine.

The total imaging time for covering the whole body in five bed positions averages to 25-30 min, including the preparation time for MR sequences.

Cases primarily referred for PET/MRI also had a dedicated pre- and post-contrast MRI of the region of interest with simultaneous PET acquisition followed by post-contrast axial T1W image for the brain and axial 3D volume interpolated breath hold examination (VIBE; TR = 3.24 ms, TE = 1.23 ms, FA = 9°, FOV = 400 mm, matrix = 1.7 × 1.3 × 4.0, TA = 15 sec, slice = 60, thickness = 4 mm) covering the whole body in five bed positions. Additional 20 min were used for regional MR study with contrast and 1 min 15 sec for the acquisition of post-contrast whole body VIBE sequence in five bed positions.

The average total imaging time for the entire whole body and regional examination was 1h. The acquired images were then composed and transferred to SYNGO via platform (Siemens) and evaluated using the mMR general workflow. Following are certain illustrated exemplary case studies done with simultaneous PET/MR.

Cases 1 and 2

Case 1

A 46 year-old male diagnosed and treated for T-cell non-Hodgkin's lymphoma in January 2009 suffered a disease relapse in June 2012. WB FDG PET/CT done elsewhere showed extensive supra and infra-diaphragmatic nodes and the patient was put on chemotherapy. During the course of treatment, he developed fever with an episode of loss of consciousness, and in view of the progressive course of disease, a CNS relapse was suspected. Since the patient was due for follow-up assessment of the disease load, in view of the brain symptoms, he was referred for FDG PET/MRI instead of ordering PET/CT and contrast MRI brain separately.

PET/MRI revealed extensive supra- and infra-diaphragmatic lymph node enlargement with increased FDG uptake

and showed disease progression from previous PET/CT study. In addition, multiple predominantly rim-enhancing conglomerating cystic lesions with tracer uptake along its rim suggesting viable tissue were seen in bilateral cerebral parenchyma. MR images further showed altered fluid content showing restricted diffusion on diffusion-weighted imaging (DWI) suggesting cerebral abscesses rather than lymphoma deposits [Figures 1A-G]. Following a course of steroids, a follow-up study was done after 6 weeks which revealed near-complete (>90%) regression of supra- and infra-diaphragmatic nodes with paradoxical increase in the rim-enhancing parenchymal brain lesions and the patient was subjected to brain biopsy which confirmed abscess on histopathology with *Nocardia asteroides* as the causative agent.

Rim-enhancing cystic brain lesions have been reported in lymphoma in immunocompromised patients,[3] and the rim enhancement on MRI is perhaps due to the presence of central necrosis. This area of central necrosis on MRI usually reveals increased apparent diffusion coefficient (ADC) value, appearing hyperintense on ADC maps. However, in the case under discussion, DWI revealed restricted diffusion in the center of lesions with lower ADC values and appearing hypointense on the ADC maps, suggesting the possibility of abscess[4] which was subsequently confirmed histopathologically.

Case 2

A 60 year-old male was diagnosed and surgically treated for moderately differentiated squamous cell carcinoma of the right lung with no adjuvant treatment. After a symptom-free interval of 6 months, he developed headache, dysarthria, and weakness of right side of the body, and was suspected of having brain metastases. Patient was referred for PET/CT of the whole body and a complementary simultaneous

FDG PET/MRI of the whole body including brain was also acquired.

There was evidence of disease recurrence in the lung on both PET/CT and PET/MRI with discrete metabolically active mediastinal nodes. In addition, a rim-enhancing cystic lesion was noted in the pons on both CT and MR, with an anterior enhancing mural nodule showing increased FDG uptake and the partially effacing the perimesencephalic and the prepontine cistern [Figure 2]. On DWI, the central necrotic component of the lesion revealed increased ADC values, appearing hyperintense on the ADC maps which favored necrosis[4] and, hence, brain metastasis as a diagnostic possibility. Stereotactic decompression of the cystic lesion and biopsy revealed metastasis on histopathology.

In cases 1 and 2, the pattern of FDG uptake with metabolically active rim and photopenic central area is nonspecific and could be characterized as abscess in case 1 and metastatic lesion in case 2 owing to their behavior on DW-MRI. The MR correlate in both these cases supplemented the information provided by PET to arrive at a diagnosis in one-shop examination.

Case 3

A 32 year-old female presented with a gradually progressive right neck swelling since 4 months. Wedge excision biopsy revealed poorly differentiated metastatic carcinoma. Patient was referred for WB PET/CT study to look for a primary site. In addition, a complementary WB FDG PET/MRI was done after the PET/CT. WB PET/CT and WB PET/MRI revealed metabolically active right nasopharyngeal thickening [Figure 3A and B] as the possible primary site and metabolically active bilateral cervical and retropharyngeal nodes which were metastatic [Figures 3C
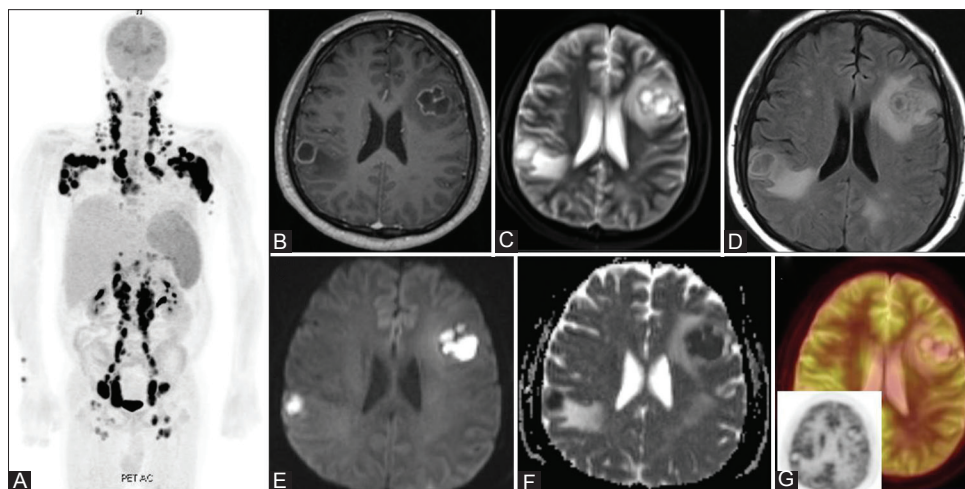

Figure 1 (A-G): 46 yr old male with relapsed T-cell NHL (A) MIP PET image of the whole body showing extensive supra and infradiaphragmatic lymphadenopathy (B) Post-contrast T1W image reveals rim enhancing lesions in brain (C) STIR axial image reveals central hyperintensity suggestive of fluid. (D) FLAIR axial image reveals mild associated perilesional edema (E) DWI axial image (b=1000) reveals central hyperintensity on high b value image with restricted diffusion on the corresponding ADC map (F). (G) Corresponding fused PET/MR image and PET AC axial (insert) reveals tracer uptake along the margins

and D].In addition, MRI revealed ill-defined marrow changes involving the pterygoid plates [Figure 3E] with mild tracer uptake suggesting involvement, not appreciable on the CT images. Also, enhancing perineural thickening was seen in the right foramen ovale extending intracranially in the right cavernous sinus region [Figure 3E] which was also not discernable on CT images. A focal marrow lesion was identified in the lateral mass of C1 vertebral body with mild tracer uptake identified retrospectively on PET images and was possibly metastatic [Figure 3F]. No identifiable lesion was seen on the corresponding CT images.

Nasopharyngeal carcinomas not only have the propensity for being locally advanced at presentation including intracranial extension by either eroding the skull base or perineural extension through the neural foramina in the skull base when the disease is staged as T4,[5] they may also be metastatic at presentation in about 5-8%of cases, with the common sites being regional nodes, bones, lung, liver, and retroperitoneal nodes.[6]

MRI is an established modality for evaluating the extent of head and neck malignancies and supersedes CT in delineating lesions better because of its excellent soft tissue contrast and delineates its local extent better than any other modality, detects marrow lesions much better (with or without cortical involvement), and can detect unsuspected perineural intracranial extension.

In this case, an apparent T2N2 disease was upstaged to T4N2M1 due to the supplemental information from the PET/MR which also altered the disease prognosis.

Case 4
A 59 year-old female presented with lumpiness in the left breast. Conventional mammography revealed dense breasts. Ultrasound (USG) of the breast revealed discrete hypoechoic mass with central necrosis in the left axilla which possibly was an axillary node with no definitive mass in the breast. USG-guided fine needle aspiration cytology (FNAC) was done which revealed metastatic duct carcinoma. Patient was referred for WB FDG PET/CT and breast MRI. Complementary simultaneous PET/MRI was performed after the WB PET/CT, which included a WB PET/MRI and dynamic contrast-enhanced breast MRI (DCE-MRI) using MR four-channel breast coil with simultaneous PET acquisition.

WB PET/CT revealed an FDG-avid left axillary node (SUV max 11.3) with an ill-defined area of tracer uptake (SUV max 3.2 vs. 2.6 in the contralateral normal breast) in
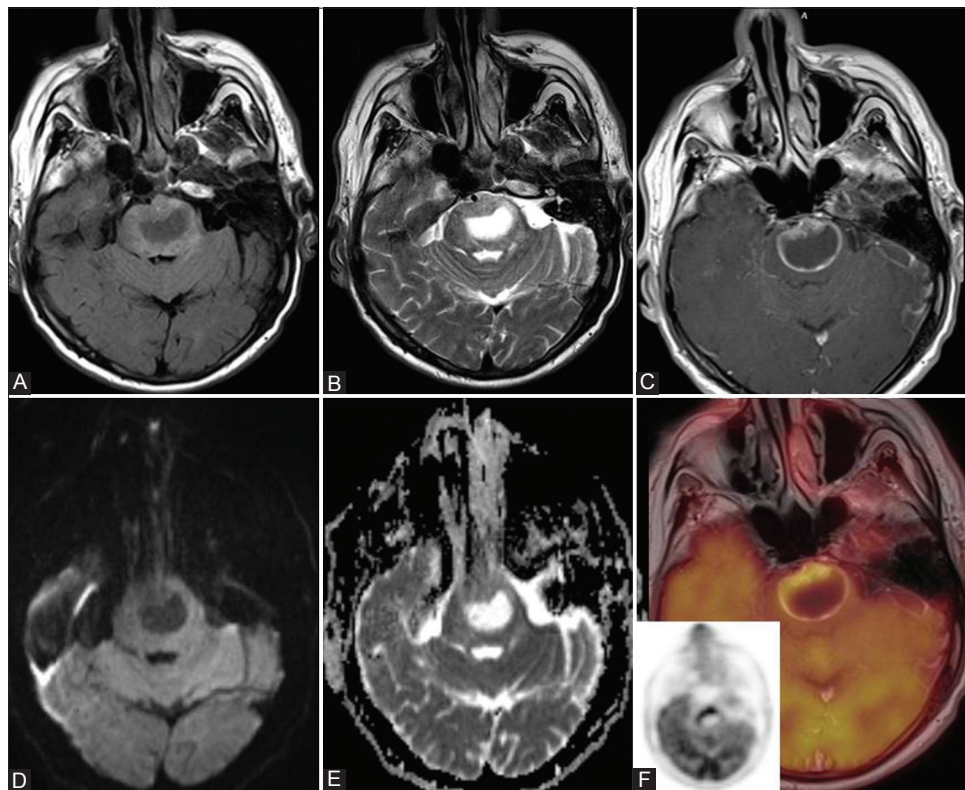

Figure 2 (A-F): 60 yr old male with carcinoma lung with CNS symptoms (A) FLAIR axial image revealed an altered intensity lesion in the pons. (B)T2W axial image reveals central hyperintensity in pontine lesion suggesting fluid. (C) Post-contrast T1W image reveals rim enhancing pontine lesion with eccentric enhancing soft tissue component. (D) DWI axial image(b=1000) reveals suppression of the central hyperintensity on high b value image with no restricted diffusion on the ADC map (E). (F) Corresponding fused PET/MR image and PET AC axial (insert) image reveals tracer uptake along the enhancing component

the retroareolar region of the left breast [Figure 4A and B].There was no evidence of metabolically active metastatic disease elsewhere in the body. WB FDG PET/MRI including the DCE-MRI of the breast revealed large area of non-mass-like segmental enhancement in the upper outer quadrant, spanning the entire breast depth and reaching upto the retroareolar region, with ill-defined FDG uptake representing the breast primary [Figure 4C] and an FDG-avid left axillary node [Figure 4D] and discrete subcentimeter intramammary nodes, simultaneously ruling out metastatic disease elsewhere in the body.

DCE-MRI of the breasts over the past decade has gained widespread acceptance for the preoperative evaluation of the true extent of primary disease in the breasts and has been reported to have multifocality and multicentricity in 6-34% of cases[7] with already proven malignancy in one breast. Simultaneous PET/MRI in this case as a single-shop examination provided exquisite details of the primary lesion in the breast MRI, which may have an impact on the surgical planning and provide a complete and comprehensive evaluation of nodal and distant metastatic status.

Case 5

A 60 year-old male patient with obstructive jaundice presented for work-up. USG of the upper abdomen revealed a mass in the porta hepatis with biliary dilatation. An USG-guided FNAC revealed cholangiocarcinoma. Patient was referred for a WB PET/CT examination. Complementary simultaneous PET/MRI was done subsequent to the PET/CT examination. PET component of both PET/CT and PET/MRI revealed a metabolically active mass in the porta hepatis with biliary obstruction [Figure 5AI–VI] and no demonstrable metabolically active metastasis in the remaining whole body and no identifiable lesion anywhere else in the WB contrast-enhanced CT. Besides providing the exquisite biliary anatomy on Magnetic resonance choliangopancreatography [Figure 5B], two subcentimeter size lesions could be identified in segment VI of liver on DW-MRI [Figure 5C]. Retrospective evaluation of contrast-enhanced CT revealed no definitive discernable lesion corresponding to the lesions detected on MR diffusion images, while mild tracer uptake could be demonstrated in relation to these lesions on PET on retrospective review. The patient was subjected to biliary stenting to relieve the obstruction before institution of definitive treatment subsequent to which he developed biliary leak for which he underwent laparotomy and the tumor was debulked. Also, peroperatively, the subcentimeter segment VI lesions could be identified on intraoperative USG and proved to be metastatic.

DWI is not only sensitive in detecting small hepatic lesions not identified on routine MR imaging sequences but also helps in lesion characterization using the ADC values.[8] In this case, additional hepatic lesions detected unambiguously on DWI were proven as being metastatic.
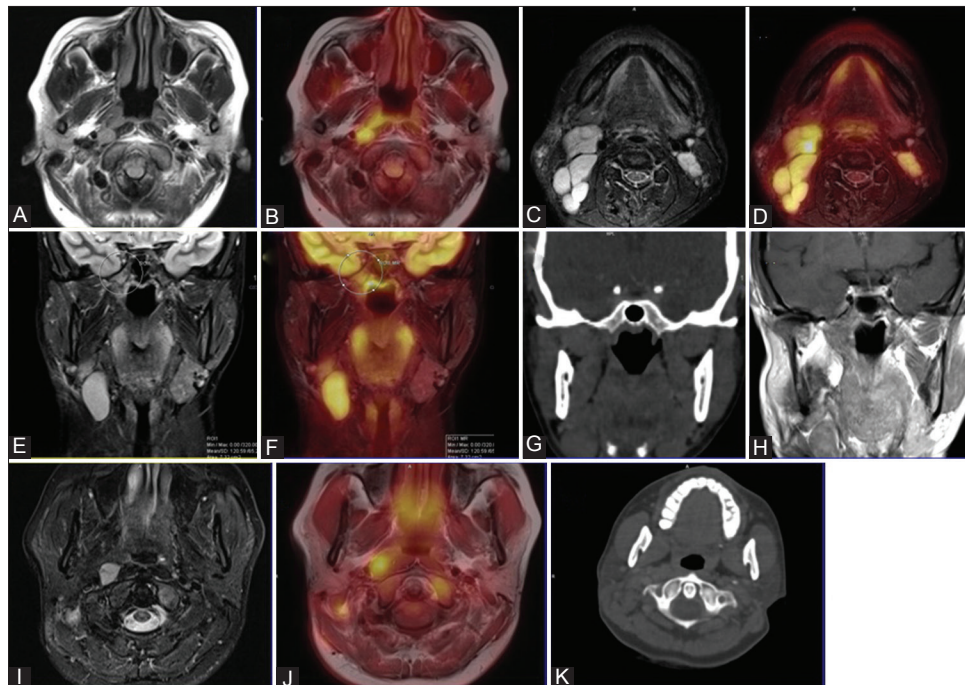
Figure 3 (A-K): 32 yr female with metastatic cervical lymphadenopathy (A, B) Post-contrast T1W (A) and PET/MR fused image (B) reveals enhancing metabolically active thickening in the right lateral wall of nasopharynx along with a confluent right lateral retropharyngeal node. FLAIR axial image reveals gliotic changes at the operated site. STIR axial (C) PET/MR fused image (D) reveals metabolically active bilateral cervical nodes. STIR coronal (E) PET/MR fused coronal (F) image reveals marrow changes in the right pterygoid plate with mild tracer uptake (arrows) (G) CT coronal image at the corresponding level with no discernible lesion in the pterygoid plates. (H) Post-contrast T1W coronal image reveals enhancing perineural thickening in the right cavernous sinus region. STIR axial (I) and PET/MR fused (J) image reveals marrow lesion in the left lateral mass of atlas vertebra with mild tracer uptake (arrows) . No identifiable lesion on the corresponding CT image (K)
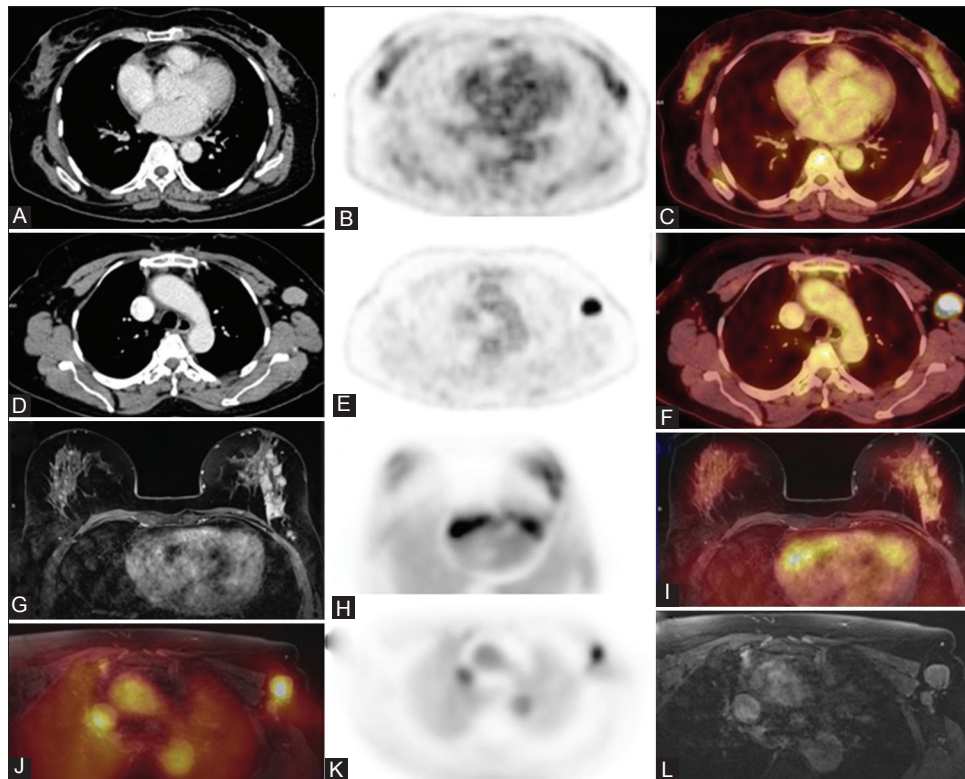
Figure 4 (A-L): 59 yr old female with vague lumpiness in the left breast. CT axial (A) PET of PET/CT axial (B) PET/CT fused image (C) reveals ill-defined tracer uptake in the left breast (arrow) CT axial (D) PET of PET/CT axial (E) PET/CT fused image (F) reveal a metabolically active right axillary node. 1st minute dynamic post-contrast fat suppressed gradient echo sequence in axial planes with patient in prone position (G) PET (H) PET/MR fused (I) reveals clumped non mass-like enhancement in the left breast spanning the entire breast depth with heterogenous tracer uptake. Axial fat suppressed T1W image (J), PET (K) and PET/MR fused (L) reveals a metabolically active left axillary node
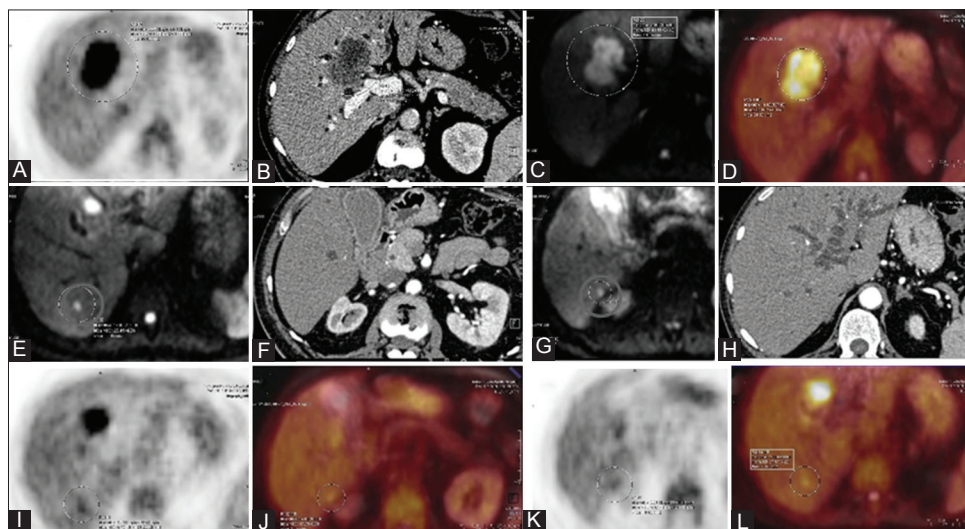

Figure 5 (A-L): 60 year old male with obstructive jaundice. Axial PET (A) Axial post-contrast CT (B) Diffusion weighted axial MR image (C) PET/MR fused (D) image reveals a metabolically active mass at the porta hepatis. Axial diffusion weighted image (E, G) reveals two discrete small altered intensity lesions in segment VI (red circle) not identified on corresponding post-contrast axial CT images (F, H) Retrospectively faint tracer uptake is identified on the corresponding PET (I, K) and fused PET/MR (J, L) images

Case 6

A 63 year-old male presented with multiple skeletal metastases with unknown primary. Patient was referred for WB PET/CT to look for a possible primary site. A complementary WB FDG PET/MRI was also done after the PET/CT.

Both PET/CT and PET/MR revealed multiple metabolically active osseous metastases [Figures 6A and B] including a metabolically active destructive soft tissue mass involving the right innominate bone. No FDG-avid lesion was noted elsewhere in the body to suggest primary

site. However, a focal lesion appearing hypointense on T2W images on MRI [Figure 6C] and showing restricted diffusion on DWI was seen in the left peripheral gland of prostate [Figure 6D]. It did not reveal any increased FDG uptake [Figure 6E]. No discrete lesion was identified on the corresponding CT image [Figure 6F]. Transrectal USG-guided biopsy of the prostate revealed prostatic adenocarcinoma.

MRI is the modality of choice for imaging the prostate for diagnosis and evaluating the exact local extent of disease in prostate cancer, while CT has a limited role. Highest diagnostic accuracy (sensitivity reaching upto 80% and specificity reaching upto 97%) has been reported by combining various MR attributes, viz., T2, DWI, and DCE-MRI. FDG PET has been reported to have a limited role in the primary staging of prostatic adenocarcinomas. However, 11C choline PET/CT has shown improved results in conjunction with MRI.[9]

Nevertheless, PET/CT and MRI are performed separately for whole body and local disease evaluation, respectively. With simultaneous PET/MRI coming into the diagnostic armamentarium, it may be a primary modality for the evaluation of prostatic carcinomas as a single examination in future. Use of specific PET tracers may further expand its utility in primary staging of prostatic cancer.

Case 7

A 68 year-old male presented with swelling in relation to the left 10th rib. He was evaluated elsewhere and diagnosed as having plasmacytoma of the rib on histopathology and received radiotherapy for the same. After a symptom-free interval of 2 months, he developed diplopia and underwent a contrast MRI of brain which revealed soft tissue thickening in relation to the left cavernous sinus, presumed to be a meningioma. Subsequently, he underwent WB FDG PET/MRI to assess the disease status in the entire body including brain. PET/MRI revealed residual soft tissue
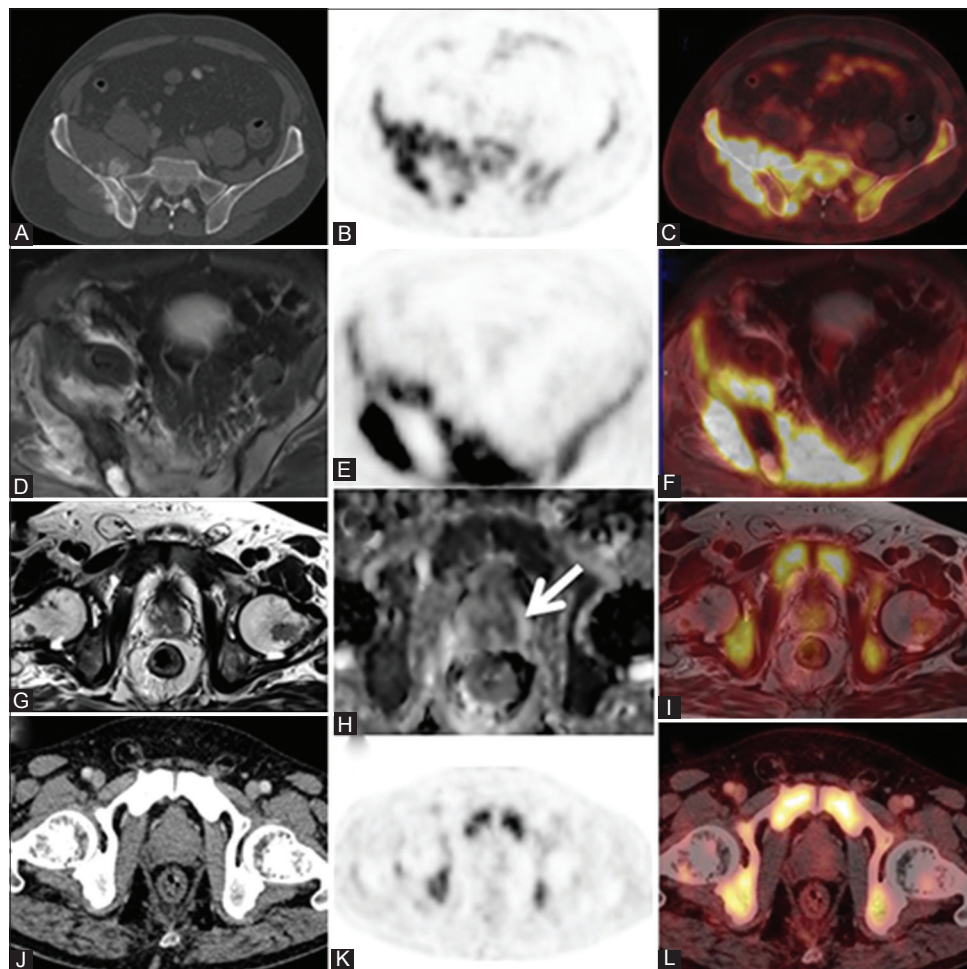

Figure 6 (A-L): 63 year old male with multiple skeletal metastasis and unknown primary. Axial CT (A) PET of PET/CT axial (B), PET/CT axial (C) reveal metabolically active lesion involving the right iliac bone with periosteal reaction. STIR axial (D) PET of PET/MR axial (E) PET/MR fused (F) reveal a metabolically active mass involving the right iliac bone and sacrum. High resolution T2W axial image reveals a focal hypointense lesion in the left peripheral gland (G) ADC map (H) reveals a focal area of restricted diffusion corresponding the lesion seen on T2W images (arrow). No demonstrable FDG uptake is seen corresponding to the prostatic lesion seen on MR on the PET/MR fused image (I). No identifiable lesion seen on corresponding (J) CT axial (K) PET of PET/CT (L) fused PET/CT images

thickening in relation to the left 10th rib with no significant tracer uptake. Soft tissue thickening in relation to the left cavernous sinus was non–FDG-avid and partially encasing the cavernous carotid artery, and was the cause of his present symptoms. In addition, focal marrow lesions with mild tracer uptake (SUV max: 2.03) were identified in the left parietal bone and the lateral end of left clavicle with possible pathological fracture [Figure 7]. In view of the history of plasmacytoma, these osseous lesions and lesion in relation to the cavernous sinus were considered to be a part of same disease process and labeled as multiple myeloma. The patient underwent radiotherapy for the cavernous sinus lesion and showed dramatic improvement in his symptoms.

Shrott *et al.*[11] compared PET/CT with WB MRI in patients with biopsy-proven multiple myeloma. They reported higher sensitivity (68% vs. 59%) and specificity (83% vs. 75%) for MRI than PET. In our patient, additional lesions could be identified on MRI, which changed the diagnosis from plasmacytoma to multiple myeloma and also directed appropriate early treatment.

Case 8

A 55 year-old male operated for carcinoma of the hepatic flexure of colon infiltrating into the adjoining liver underwent right hemicolectomy with wedge resection of the involved liver and was found to have rising carcinoembryonic antigen CEA on routine follow-up. USG of the abdomen was unremarkable. WB simultaneous FDG PET/MRI revealed a focal area of increased tracer uptake in the resected liver bed, which was inseparable from the physiological bowel activity in the adjoining bowel loop.[12] The lesion could be clearly identified on MR sequences separate from the bowel and lying in segment VI of the liver in the resected liver bed, suggesting local recurrence [Figure 8]. The ileo-transverse

anastomotic site was free. There was no evidence of metastasis elsewhere in the body.

Increased tracer uptake in a previously operated site, as in this case, suggested possible disease recurrence, but the true localization of the activity which was inseparable from the adjoining bowel could be done accurately due to improved display of anatomy with MR, and superior co-registration of simultaneously acquired PET and MR data aided precise localization of this activity to the liver that changed the management of this case.[2]

Case 9

A 58 year-old post-menopausal female was diagnosed and treated for non-keratinizing squamous cell carcinoma of the cervix stage IIIb. She received concurrent chemoradiation 1 year back and was on follow-up. She presented to our hospital with complaints of bleeding per vaginum since last 3 months. Cervical biopsy done elsewhere showed radiation necrosis. Simultaneous FDG PET/MRI done revealed a heterogeneously enhancing necrotic cervical mass on MRI with mild diffuse tracer uptake (SUVmax: 4). The mass exhibited areas of diffusion restriction with low ADC value [Figure 9]. Though FDG PET has been reported to have high sensitivity and specificity for detecting cervical cancer recurrences,[13] in our case, the PET showed equivocal diffuse tracer uptake which could be either due to inflammation or disease, but the MR component of the simultaneous PET/MRI suggested possibility of disease recurrence and prompted tissue diagnosis. A guided biopsy from the cervical mass was done which revealed poorly differentiated carcinoma on histopathology. In this case, MRI emphasized the possibility of disease recurrence which was proven early and aided in clinical management.
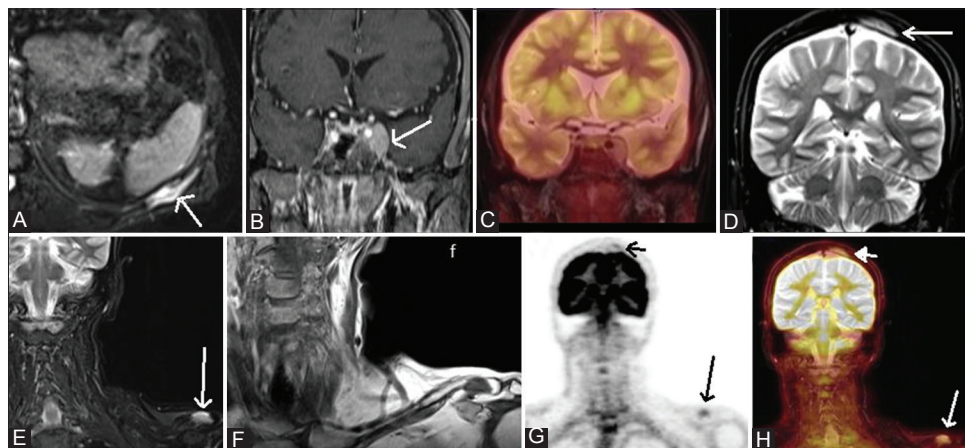

Figure 7 (A-H): 68 yr male with plasmacytoma of left 10th rib post RT with diplopia. (A) STIR axial image reveals altered intensity in left 10th rib (arrow). (B) Post-contrast T1W coronal VIBE image reveals an enhancing soft tissue lesion in the Lt. cavernous sinus(arrow). (C) PET/MR fused image with no tracer uptake in Lt. cavernous sinus. (D) STIR coronal image reveals marrow lesion in Lt. parietal bone(arrow). (E) Coronal STIR and (F) Coronal T1W reveals marrow lesion in Lt. clavicle(arrow). (G) PET AC coronal (H) PET/MR fused coronal image reveals mild tracer uptake in Lt. clavicle (arrow) and Lt. parietal bone (small arrow)

Discussion

The advent of truly integrated PET/MRI systems is expected to give a boost in the emerging field of molecular imaging because of the availability of complementary anatomic and biologic information. Initial studies with simultaneous PET/MRI suggest its feasibility[14,15] and the potential for multiple clinical applications, mainly due to better correlation of PET findings to anatomy owing to simultaneous acquisition, besides providing lower radiation exposure which is

Figure 8 (A-D): 55 year old male operated for Ca hepatic flexure of colon presented with rising CEA. (A) PET of PET/MRI revealed a focal area of increased tracer uptake (arrow) inseparable from the adjoining bowel activity. (B) Post-contrast VIBE coronal image reveals a centimetre sized enhancing lesion in segment VI of the liver (arrow) in the operated bed and adherent small bowel loop lying close to it. (C) PET/MR fused image precisely localises the focal FDG activity to the enhancing liver lesion (arrow). (D) Non-contrast TruFISP axial image reveals an altered intensity lesion identified separate from the bowel

especially important in pediatric patients and for follow-up studies. Catalano *et al.* found PET/MRI to be extremely useful in identifying more hepatic, renal, and bony lesions.[16] It appears to be highly accurate in T-staging of those malignancies for which MRI has been conventionally favored, such as tumors of the head and neck and pelvis where soft tissue resolution of MRI outperforms CT. Evaluation of distant metastases could benefit from accuracy of MRI in the brain and the liver.[17] However, several challenges are evident mainly with regard to validation of PET quantitation accuracy derived from MRI-based attenuation correction. Many recent studies have, however, shown that attenuation-corrected PET data from PET/CT and PET/MR obtained using the Dixon sequences correlate well both qualitatively and quantitatively (SUV) and that there is no significant difference between the two modalities as far as lesion detection is concerned.[18,19] Another major challenge that remains is optimization of protocols for different body regions which can provide good diagnostic quality images along with PET acquisition within a reasonable study period. The average imaging time in our cases including WB MRI with PET and pre- and post-contrast diagnostic imaging of the region of interest with simultaneous PET acquisition was 1 h.

Our initial experience of few cases with simultaneous PET/MRI indicates the potential use of this hybrid modality in cancer imaging. Although the current literature focuses on ^{18}F-FDG, more specific tracers should be addressed in the future which, along with several functional MR parameters (e.g. DWI, DCE-MRI, and MR spectroscopy), is likely to exponentiate potential clinical applications for both oncology and non-oncology cases. Though still in its infancy, simultaneous PET/MRI appears to be a promising imaging modality and larger studies are needed to be undertaken to establish its full diagnostic potential.
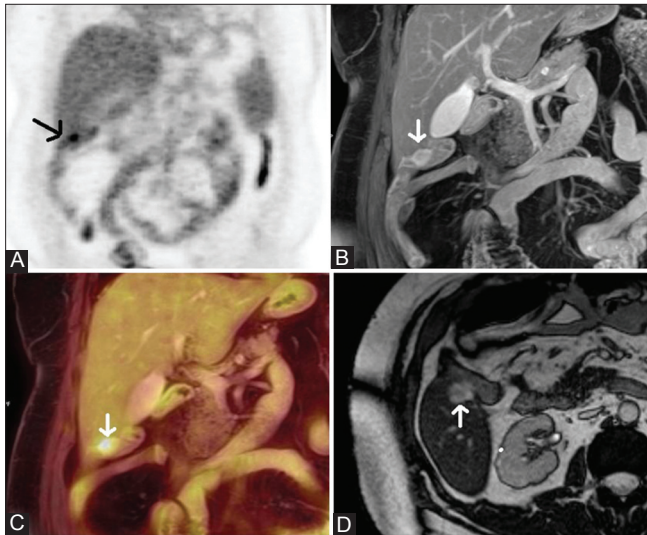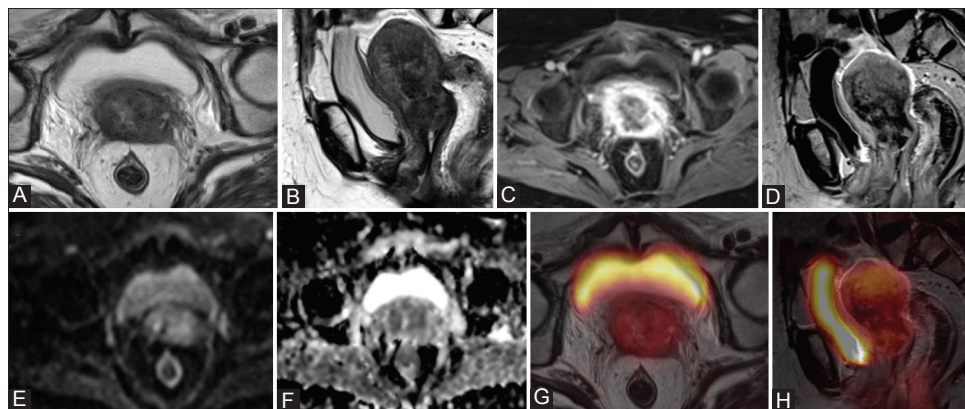

Figure 9 (A-H): 58 year old female received radiotherapy for carcinoma of cervix stage IIIb. Presented with bleeding per vaginum after a symptom free interval of one year. Cervical biopsy elsewhere was negative.(A,B) T2W axial and sagittal image reveals a mass in the cervix with involvement of the uterine corpus. Post-contrast VIBE axial (C) and post-contrast T1W sagittal image (D) reveal heterogenous enhancement in the cervical mass. (E) DWI axial (b value=1000) and corresponding ADC map (F) reveal focal areas of restricted diffusion in the cervical mass. (G,H) PET/MR fused images reveal mild tracer uptake

References

1. Antoch G, Saoudi N, Kuehl H, Dahmen G, Mueller SP, Beyer T, *et al*. Accuracy of whole-body dual modality fluorine-18-2-fluoro-deoxy-D-glucose positron emission tomography and computed tomography (FDG-PET/CT) for tumor staging in solid tumors: Comparison with CT and PET. J Clin Oncol 2004;22:4357-68.

2. Brendle CB, Schmidt H, Fleischer S, Braeuning UH, Pfannenberg CA, Schwenzer NF. Simultaneously acquired MR/PET images compared with sequential MR/PET and PET/CT: Alignment Quality. Radiology 2013;268:190-9.

3. Rakheja R, DeMello L, Chandarana H, Glielmi C, Geppert C, Faul D, *et al*. Comparison of accuracy of PET/CT and PET/MR spatial registration in multiple metastatic lesions. AJR Am J Roentgenol 2013;201:1120-3.

4. Johnson BA, Fram EK, Johnson PC, Jacobwitz R. The Variable MR appearance of Primary Lymphoma of the Central Nervous System: Comparison with Histopathologic features. AJNR Am J Neuroradiol 1997;18:563-72.

5. Chang SC, Lai PH, Chen WL, Weng HH, Ho JT, Wang JS, *et al*. Diffusion-Weighted MRI features of brain abscess and cystic or necrotic brain tumors: Comparison with conventional MRI. Clin Imaging 2002;26:227-36.

6. Li L, Yuan W, Liu L, Cui C. MRI detected Cranial nerve involvement in Nasopharyngeal carcinoma, carcinogenesis, diagnosis, and Molecular targeted Treatment for nasopharyngeal carcinoma, Dr. Shih-Shun Chen, editor., ISBN: 978-953-307-867-0In Tech. Available from: http://www.intechopen.com/books/ carcinogenesis-diagnosis-and-molecular-targeted-treatment-for-nasopharyngeal- carcinoma/ mri-detected-cranial-nerve-involvement-in-nasopharyngeal-carcinoma [Last accessed on 2013 Oct 07].

7. Tian YM, Zeng L, Wang FH, Liu S, Guan Y, Lu TX, *et al*. Prognostic factors in nasopharyngeal carcinoma with synchronous liver metastasis: A retrospective study for the management of treatment. Radiat Oncol 2013;8:272.

8. Bruegel M, Holzapfel K, Gaa J, Woertler K, Waldt S, Kiefer B, *et al*. Characterisation of focal liver lesions by ADC measurements using a respiratory triggered DW single shot echoplanar imaging technique. Eur Radiol 2008;18:477-85.

9. Park H, Wood D, Hussain H, Meyer CR, Shah RB, Johnson TD, *et al*. Introducing parametric fusion PET/MRI of primary prostate cancer. J Nucl Med 2012;53:546-51.

10. Shortt CP, Gleeson TG, Breen KA, McHugh J, O'Connell MJ, O'Gorman PJ, *et al*. Whole body MRI versus PET in assessment of Multiple Myeloma Disease activity. AJR Am J Roentgenol 2009;192:980-6.

11. Shreve PD, Anzai Y, Wahl RL. Pitfalls in oncologic diagnosis with FDG PET imaging: Physiological and benign variants. Radiographics 1999;19:1 61-77.

12. Patel NC, Nazir SA, Khan Z, Gleeson FV, Bradley KM. 18 F-FDG PET/CT of cervical carcinoma. AJR Am J Roentgenol 2011;196:1225-33.

13. Von Schulthess GK, Sclemmer HP. A look ahead: PET/MR versus PET/CT. Eur J Nucl Med Mol Imaging 2009;36:S3-9.

14. Delso G, Fürst S, Jakoby B, Ladebeck R, Ganter C, Nekolla SG, *et al*. Performance measurements of the Siemensm MR integrated whole-body PET/MR scanner. J Nucl Med 2011;52:1914-22.

15. Catalano OA, Rosen BR, Sahani DV, Hahn PF, Guimaraes AR, Vangel MG, *et al*. Clinical impact of PET/MR imaging in patients with cancer undergoing same-day PET/CT: Initial experience in 134 patients-a hypothesis-generating exploratory study. Radiology 2013;269:857-69.

16. Buchbender C, Heusner TA, Lauenstein TC, Bockisch A, Antoch G. Oncologic PET/MRI, Part 1: Tumors of the Brain, Head and Neck, Chest, Abdomen, and Pelvis. J Nucl Med 2012;53:928-38.

17. Drzezga A, Souvatzoglou M, Eiber M, Beer AJ, Fürst S, Martinez-Möller A, *et al*. First Clinical Experience with Integrated Whole-Body PET/MR: Comparison to PET/CT in Patients with Oncologic Diagnoses. J Nucl Med 2012;53:845-55.

18. Al-Nabhani KZ, Syed R, Michopoulou S, Alkalbani J, Afaq A, Panagiotidis E, *et al*. Qualitative and Quantitative Comparison of PET/CT and PET/MR Imaging in Clinical Practice J Nucl Med 2014;55:88-94.

19. Heusch P, Buchbender C, Beiderwellen K, Nensa F, Hartung-Knemeyer V, Lauenstein TC, *et al*. Standardized uptake values for [18F] FDG in normal organ tissues: Comparison of whole-body PET/CT and PET/MRI. Eur J Radiol 2013;82:870-6.